Interfacial Stress in a Carbon-to-Metal Bond Joint under Thermal Shock Loading

J.H. You

(Submitted 28 July 1997; in revised form 1 September 1997)

The duplex bond joint consisting of a metallic substrate armored with carbon-base materials is a promising candidate configuration for application to high heat flux operations. When a bond joint is subjected to thermal loadings, significant thermal stresses may develop due to mismatch of the thermal expansion coefficients. Stress intensification occurs near the free surface edge of the interface, sometimes showing singularity. The singular stress fields are critical for understanding the loading nature of the bond interface in a joint system.

In this paper, thermal stresses in the bond interface of a carbon-to-molybdenum joint element were investigated. A high heat flux (HHF) pulse was assumed as the reference load history to simulate the thermal shock condition. The thermomechanical behavior was described quantitatively in terms of the stress intensity factor.

The stress solutions of the singular field computed by the theoretical approach showed a good agreement with the numerical results of the finite element analysis. The stress intensity factor of the singular stress fields near the free surface edge of the interface showed a time variation similar to that of the bulk stress. The temperature gradient induced by the transient HHF load affected the overall interfacial stress only slightly.

Keywords carbon copper, composites, high heat flux, stress

1. Introduction

There is increasing use of joined refractory and metallic material combinations exposed to a widening range of temperatures. In particular, they have major applications in high heat flux (HHF) areas such as fusion reactors, power plants, and hypersonic vehicles, including space shuttles. Brazing, friction welding, and diffusion bonding have been attractive joining technology to fabricate such joint structures. A duplex material configuration consisting of a metallic substrate armored with carbon-base materials can fulfill dual material requirements during HHF operations. The carbon armor withstands significant heat flux as well as thermal shock without causing serious material degradation at high temperature, whereas the metallic substrate supports the cooling body and transfers the heat from the carbon tiles to the heat sink, maintaining reasonable peak surface temperature.

However, difficulties can arise in the manufacturing or in the service of the bond joints. It has been reported from many of the thermal loading experiments conducted on joint components that failures occur mostly near or at the bond interface of the joints (Ref 1-6). The debonding of a joint interface can also occur, even during the joining process. During the joining process, as the materials are cooled from the bonding temperature to room temperature, significant residual stresses may develop. These stresses are primarily due to mismatch of the thermal expansion coefficients. When a brazed joint is subjected to additional thermal loads, the resulting thermal stresses will be superimposed onto the residual stress fields.

Reliability demands on equipment employing carbon-to-metal bonds require a more complete understanding of structural integrity characteristics, because the carbon-base materials are in general brittle.

For the investigation of this issue, thermal stresses in the bond interface of a carbon-to-molybdenum bond element were analyzed. Both secondary stresses and residual stress were calculated using a finite element method. In this paper, the thermomechanical behavior of the bond interface under a transient HHF shock loading is discussed. A theoretical treatment of singular stress fields near the free surface as well as bulk stress is presented.

2. Theoretical Models

The simple beam theory can be used to calculate the stresses in the bulk region of a brazed joint (Ref 7, 8). In this model, it is assumed that the longitudinal length of the bond strip is sufficiently larger than the thickness of each layer. Under this limitation, the solution is valid only for the region distant from the edge boundary (Saint Venant's effect). The stress solution based on the beam theory is uniaxial and dependent on the distance from the neutral axis of the strip.

The level of the thermal stresses near the interface is normally higher than that of other bulk regions and increases rapidly near the free surface edge of the interface (Ref 3, 7, 9-11). The stress intensification occurring in this region can be singular for certain material combinations and wedge geometries (Ref 12). The singular stress fields are generated due to nonuniform deformation of the interface region at the free surface, whereas the bulk stresses are mainly caused by the misfit of the thermal expansion coefficients.

J.H. You, Institute for Materials in Energy Systems, Forschungszentrum Jülich, EURATOM Association, D-52425 Jülich, Germany.

When the materials are brittle, cracks are often initiated in this region, leading to abrupt fracture (Ref 3, 4). Hence, the singular stress fields occurring in the bond interface are significant for understanding the loading behavior of divertor joint components.

The stress fields near the free surface edge of the interface have been extensively investigated. Several plane solutions have been given by various analytical procedures (Ref 13-19). When the stress singularity exists, the strength of the singularity is represented by the exponent of singularity. The strength of these stress singularities is affected only by the Dundurs' parameters, which are combinations of elastic constants (Ref 18). This parameter can be determined analytically (Ref 14).

It is useful to introduce a fracture mechanical parameter that relates boundary conditions to resultant stress solutions. The stress intensity factor can be taken as such a representative quantity that describes the asymptotic stress fields near the free surface edge of the interface (Ref 16, 20).

While the exponent of stress singularity remains constant for a given material combination and wedge geometry, the stress intensity factor can represent the evolution of transient loading responses. A failure criterion can be obtained from this parameter for a specific thermal loading condition.

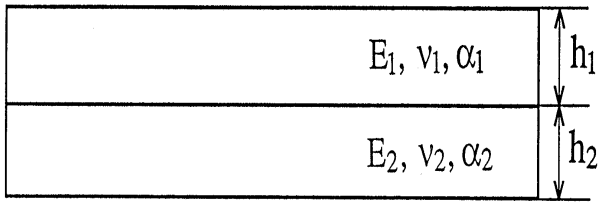

Fig. 1 Two-dimensional joint model used for Timoshenko's theory. See text for definitions.

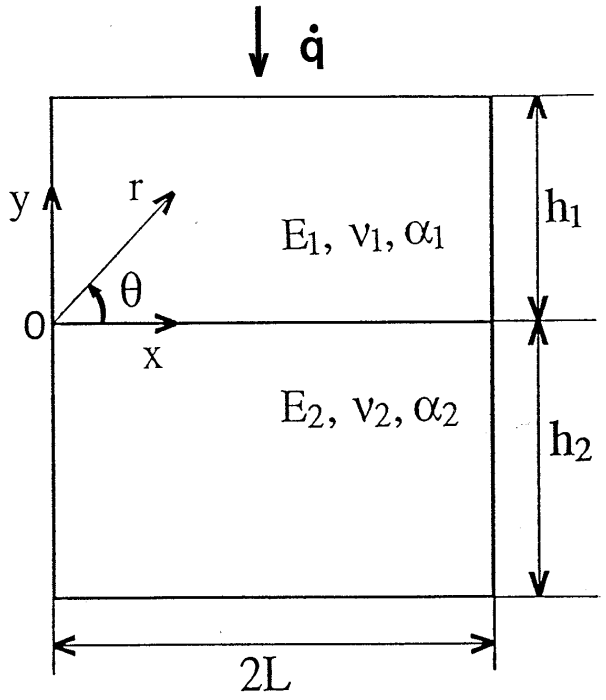

Fig. 2 Two-dimensional joint model used to analyze the interfacial stress

2.1 *Bulk Stress in a Bond Joint*

The solution for the bulk thermal stresses in a perfectly bonded joint consisting of two layered strips was given by Timoshenko (Ref 7). The model for this analysis is shown in Fig. 1, where E_i is Young's modulus, ν_i is Poisson's ratio, h_i is the thickness of each strip, and α_i is the thermal expansion coefficient. Subscript *i* denotes material 1 and material 2. The maximum stress occurring at the material interface is found to be:

$$\sigma_{max} = \frac{1}{\rho}\left[\frac{2(E_1I_1 + E_2I_2)}{h_1(h_1 + h_2)} + \frac{1}{2}E_1h_1\right] \quad \text{(Eq 1)}$$

where I_i is the moment of inertia of the individual layers and ρ is the radius of curvature of the strip. I_i is of the form:

$$I_i = \frac{h_i^3}{12} (i = 1, 2) \quad \text{(Eq 2)}$$

and ρ is given by:

$$\rho = \frac{(h_1 + h_2)\left[3(1 + m)^2 + (1 + mn)\left(m^2 + \frac{1}{mn}\right)\right]}{6(\alpha_2 - \alpha_1)\Delta T(1 + m)^2} \quad \text{(Eq 3)}$$

where ΔT is the temperature change and *m*, *n* are given by:

$$m = \frac{h_1}{h_2}, n = \frac{E_1}{E_2} \quad \text{(Eq 4)}$$

As was mentioned, the stress solution given in Eq 1 is uniaxial and there are no normal or shear stress components. For an interfacial crack of a thermally stressed bond joint, the crack extension is driven by the combination of three modes of fracture. This mixed-mode deformation of the crack tip is strongly related to the normal and shear components of the near-tip stress fields. The bulk stress level is proportional to the misfit of the thermal expansion coefficients and the temperature change. It was shown by Timoshenko that the solution depends weakly on the mismatch of the elastic modulus. The solution is valid only for elastic, isotropic materials subjected to uniform temperature change. Thus it cannot yield correct predictions for the thermal stress fields generated by HHF loadings.

2.2 *Stress State Near Free Surface Edge of an Interface*

The beam theory breaks down near the free edge of the bimaterial interface due to the deformation of the traction-free surfaces. A more rigorous analysis is needed to investigate the stress fields in this region. The model geometry used for the analysis is shown in Fig. 2.

In linear elastic fracture mechanics, the stress field near a crack tip is approximated as:

$$\sigma_{ij}(r,\theta) = \frac{K}{(2\pi r)^{0.5}} f_{ij}(\theta) \quad \text{(Eq 5)}$$

where r, θ are polar coordinates having their origin at the crack tip and $f_{ij}(\theta)$ is a function of the angle depending on the particular fracture mode.

The stress intensity factor K is considered to be a measure of the stress intensification near the singular point and has been taken as a useful criterion to predict crack extension.

Based on the fracture mechanical analogy, Munz and Yang (Ref 18) suggested that the stress state near the singular point in Fig. 2 can be described by:

$$\sigma_{ij}(r,\theta) = \frac{K}{(r/L)^{\omega}} f_{ij}(\theta) + \sigma_{ijo}(\theta) \quad \text{(Eq 6)}$$

where ω is a given wedge angle and the distance r is normalized by a characteristic length of the joint. In Fig. 2, a special geometry with an orthogonal wedge at the interface edge is considered and a perfect bond interface is assumed.

For a given wedge angle, ω, $f_{ij}(\theta)$, K, and $\sigma_{ijo}(\theta)$ are dependent on the elastic constants E and ν. In addition, the stress intensity factor K and the nonsingular term σ_{ijo} are dependent on the thermal expansion coefficient α and are proportional to the temperature difference ΔT. The order of singularity ω, the angular function f_{ij}, and the stress term σ_{ijo} can be determined analytically.

The order of singularity ω is obtained by solving the following equation:

$$\lambda^2(\lambda^2 - 1)\alpha^2 + 2\lambda^2[\sin^2(\pi\lambda/2) - \lambda^2]\alpha\beta + [\sin^2(\pi\lambda/2) - \lambda^2]^2\beta^2 + \sin^2(\pi\lambda/2)\cos^2(\pi\lambda/2) = 0 \quad \text{(Eq 7)}$$

where

α, β are Dundurs' parameter and

$$\lambda = 1 - \omega \quad \text{(Eq 8)}$$

$$\alpha = \frac{m_2 - km_1}{m_2 + km_1} \quad \text{(Eq 9a)}$$

$$\beta = \frac{(m_2 - 2) - k(m_1 - 2)}{m_2 + km_1} \quad \text{(Eq 9b)}$$

with

$$k = \frac{\mu_2}{\mu_1} \quad \text{(Eq 10a)}$$

$$m_i = 4(1 - \nu_i) \text{ (plane strain)} \quad \text{(Eq 10b)}$$

The components of the nonsingular term σ_{ijo} are:

$$\sigma_{rro} = \frac{\sigma_o}{2}(1 - \cos 2\theta) \quad \text{(Eq 11a)}$$

$$\sigma_{\theta\theta o} = \frac{\sigma_o}{2}(1 + \cos 2\theta) \quad \text{(Eq 11b)}$$

$$\tau_{r\theta o} = \frac{\sigma_o}{2}\sin 2\theta \quad \text{(Eq 11c)}$$

where

$$\sigma_o = \Delta\alpha \cdot \Delta E \cdot \Delta T \quad \text{(Eq 12a)}$$

$$\Delta\alpha = \alpha_1(1 + \nu_1) - \alpha_2(1 + \nu_2) \quad \text{(Eq 12b)}$$

$$\Delta E = \left[\frac{1}{E_1^*} - \frac{1}{E_2^*}\right]^{-1} \quad \text{(Eq 12c)}$$

$$E_i^* = \frac{E_i}{\nu_1(1 + \nu_i)} \text{ (plane strain)} \quad \text{(Eq 12d)}$$

The stress intensity factor K can be determined using the stress solution σ_{ij}^{FEM} obtained from the finite element analysis. Equation 13 shows a double logarithmic expression of Eq 6, where the stress term σ_{ij} is replaced by σ_{ij}^{FEM}:

$$\log_{10}\left[\frac{\sigma_{ij}^{FEM}(r,\theta) - \sigma_{ijo}(\theta)}{f_{ij}(\theta)}\right] = -\omega\log_{10}(r/L) + \log_{10}(K) \quad \text{(Eq 13)}$$

It can be seen that in a plot of $\log_{10}\left|\left(\sigma_{ij}^{FEM}(r,\theta) - \sigma_{ijo}(\theta)\right)/f_{ij}(\theta)\right|$ vs. $\log_{10}(r/L)$ for θ = constant, there is a straight line in the range near the singular point. The intercept of the straight line on the axis corresponds to $\log_{10}(K)$, whereas the slope of the line yields ω. Because σ_{ij}^{FEM} is obtained for a finite body under specific thermal load, the effects of finite dimension and inhomogeneity of the temperature field are included in the procedure to determine the stress intensity factor K. In contrast to this, ω and f_{ij} are independent of the thermal gradient, because these parameters are determined only for the local domain near the singular point.

It has been shown that σ_{ijo} is hardly affected by the temperture gradient at the interface (Ref 21). Therefore, the stress intensity factor K can be determined using Eq 13, even for a transient thermal loading condition that causes a nonharmonic temperature field.

2.3 *Transient Thermal Conduction*

To obtain the thermal stress and deformation field solutions, the transient temperature fields generated by HHF loading were determined applying the following boundary conditions.

It was assumed that a uniform surface heat flux of 20 MW/m^2 was deposited on the carbon protection tile surface with a pulse duration of 2 s. In the HHF simulation, radiation heat transfer was assumed to take place on the free boundaries except for the bottom face where it is ascribed to thermal isolation. This is a typical thermal loading condition in HHF loading simulations.

The governing equation for the transient heat conduction is:

$$k_i \nabla^2 T = \rho_i C_i \frac{\partial T}{\partial t} \quad \text{(Eq 14)}$$

where k_i is the thermal conductivity, ρ_i is the density, and C_i is the molar specific heat. The initial condition is:

$$T(x, y, 0) = T_i = 20\ ^\circ\text{C} \quad \text{(Eq 15)}$$

Considering the radiation heat transfer on the free surfaces, the boundary conditions are written as:

$$-k_1 \frac{\partial T(x, h_1, t)}{\partial y} = -\dot{q} + \varepsilon_1 \sigma (T^4 - T_a^4)\ (0 \le t \le 2\ \text{s}) \quad \text{(Eq 16)}$$

$$-k_1 \frac{\partial T(x, h_1, t)}{\partial y} = \varepsilon_1 \sigma (T^4 - T_a^4)\ (2\ \text{s} < 6\ \text{s}) \quad \text{(Eq 17)}$$

$$k_2 \frac{\partial T(x, -h_2, t)}{\partial y} = 0 \quad \text{(Eq 18)}$$

where h_1 and h_2 is the thickness of materials 1 and 2 in Fig. 2, $\dot{q}$ is the magnitude of the input heat flux, ε is the emissivity of the materials, σ is the Stefan-Boltzmann constant, and T_a is the ambient temperature, which is equal to the initial temperature T_i.

Interface conditions are given as:

$$T(x, 0^+, t) = T(x, 0^-, t)\ \ (0 < x < L) \quad \text{(Eq 19)}$$

$$k_1 \frac{\partial T(x, 0^+, t)}{\partial y} = k_2 \frac{\partial T(x, 0^-, t)}{\partial y}\ \ (0 < x < L) \quad \text{(Eq 20)}$$

3. Computations

The thermoelastic analysis was carried out using the finite element code ABAQUS (Ref 22). Eight-noded isoparametric quadrilateral elements were used for the thermal and stress analysis. For the calculation of crack tip stress fields, interface elements were employed to keep the crack faces from overlapping.

The two-dimensional joint model shown in Fig. 2 was used for the analysis. As an example, the geometry of $h_1 = h_2 = 10$ mm and $2L = 25$ mm was chosen. The CFC (carbon composite)-to-molybdenum alloy bond joint was selected for the materials of the armor tile (material 1) and the metallic substrate (material 2), respectively. Due to the symmetry, only the left half part was considered. The problem size of the computation models is listed in Table 1.

Some selected material properties are listed in Table 2. In numerical analysis, the temperature dependence of the material properties and material anisotropy were taken into account, whereas all the analytical parameters were calculated using constant material properties at room temperature. In addition, the anisotropic material properties were given as averaged values.

The simulation of the brazing process preceded the HHF step to generate the residual stresses on which the following secondary thermal stresses were superimposed. The stress-free reference temperature was taken as 1070 °C which was the solidus temperature of the braze metal. First, it was assumed that the CFC tile would be bonded to the TZM substrate (Mo-0.5Ti-0.1Zr) at 1070 °C. Then the joint was cooled homogeneously to room temperature, where the joint would exist in a residually stressed state.

4. Results and Discussion

4.1 *Analysis of the Temperature Field*

Figure 3 shows the reference thermal load history and the calculated temperature evolution that was applied for the further numerical and theoretical analyses.

The joint was thermally equilibrated in 4 s after the load-off point. At the end point of the load pulse, a maximum temperature gradient developed where the surface temperature reached its maximum. The temperature at the bond interface increased monotonically.

4.2 *Analysis of the Bulk Stress*

The behavior of bulk stresses at the joint interface is shown in Fig. 4. Two cases of thermal load conditions, HHF loading

Table 1 Problem size of the finite element analysis for each theoretical model

Model	Number of elements	Number of node points
Timoshenko (σ_{max})	900	2945
Yang (K)	1250	4054

Table 2 Selected material properties at room temperature

Property	2D CFC Sepcarb N112	TZM (Mo-0.5Ti-0.1Zr)
Poisson's ratio	0.14	0.32
Elastic modulus, GPa	28(//) 24 (⊥)	300
Thermal expansion coefficient, K^{-1}	1.5 (//) 2.7 (⊥)	5.3
Strength (tens./comp.), MPa	65/160 (//) 35/180 (⊥)	550 ($R_{p0,2}^{400\ ^\circ\text{C}}$) 1150 ($R_m$)
Thermal conductivity, W/mK	280 (//) 210 (⊥)	125

Source: Ref 23

and isothermal heating, are considered. The axial component of the interfacial stress at the center of the CFC side is given. This is the bond interface region where the misfit of the coefficients of the linear thermal expansion produces the maximum stress level, so the interfacial temperature curve in Fig. 3 was taken as the reference load history for the isothermal heating simulation.

The numerical result is compared to the maximum bulk stress value obtained from Timoshenkos beam theory. In the beam theory approach, a uniform temperature field was assumed, the time history of which was identical to that used for the isothermal heating simulation. There is some discrepancy between the numerical results and the values from the beam model, ranging from approximately 12.5 to 25%. This difference is mainly due to the limitations assumed in Timoshenko's model.

In the residual stress state at room temperature, the joint mostly exists in the stressed state. As the joint is heated during thermal loading, the stress reduction takes place coupled to the difference between the brazing and current temperature at the interface. It can be seen from Fig. 4 that the temperature gradient induced by the transient HHF load affects the bulk stress only slightly.

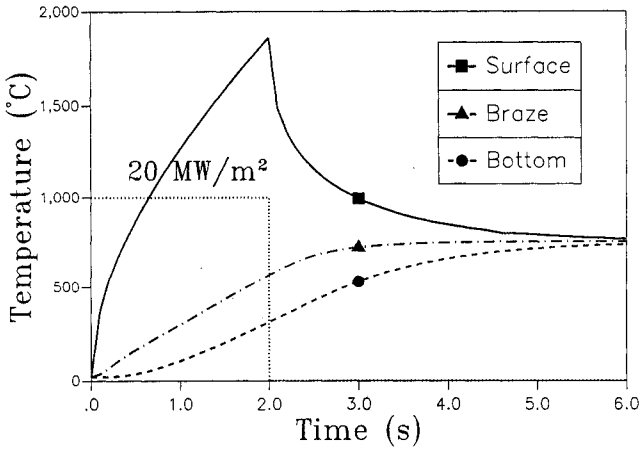

Fig. 3 Reference thermal load history and the corresponding temperature evolution applied for the numerical analysis

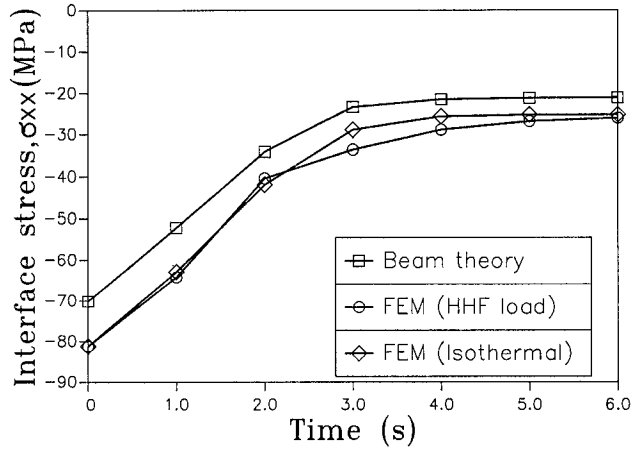

Fig. 4 Evolution of the interfacial bulk stress at the interface center

4.3 *Stress Distributions along the Bond Interface*

Figure 5 shows the residual stress distribution in the bond interface of the CFC side. The *x*-axis means the normalized *x* coordinate along the interface with the origin at its free surface edge. The corresponding finite element mesh is shown in Fig. 6. The mesh near the free surface edge of the interface was refined for the precise determination of the singular stress fields.

The axial stress component σ_{xx} parallel to the bond interface (Fig.5a) and the normal stress component σ_{yy} vertical to the bond interface (Fig.5b) are plotted. A cracked interface as well as a perfect interface were considered for the comparison. The former was assumed to have two cracks located at the free boundary and at the symmetry center. To calculate the stress field near the center crack, the symmetry axis boundary was combined with the refined mesh region. The length of the interfacial cracks was 0.5 mm, which amounts to 4% of the whole interface length.

In front of the crack tips and near the free surface edge, stress concentration is found in the form of singularities, as was predicted by the theoretical models.Compared to the bulk stress level, the rate of stress intensification is very high. In the bulk region distant from these singularities, the stress values for both interfaces coincide, which means that the interfacial cracks affect the stress fields just in the vicinity of the crack tips. Because the numerical results for the singular stress fields are normally influenced by the degree of mesh refinement, the convergence of the solutions was confirmed by optimizing the element size.

The bulk stress values of the axial component near the center of the interface agree with the results in Fig. 4. In Fig. 5(b), it is shown that the normal component of the bulk stresses is negligible, as was predicted in the beam theory. However, the normal component near the crack tips and near the free surface edge shows singular stress fields. Together with the shear stress component, it puts these regions into the multiaxial stress state.

The behavior of the singular stress field near the free surface boundary is analyzed in the following sections.

4.4 *Analysis of the Singular Stress Fields near the Free Surface Region of the Interface*

Applying the numerical stress solutions to Eq 13, the stress intensity factor *K* is obtained for the perfect interface in Fig. 2. The stress intensity factor *K* represents the complete singular stress field near the free surface edge of the interface. The calculated analytical parameters for the given joint system are as follows:

$\omega = 0.1805$
$\sigma_o = 148.1$ MPa
$f_{xx} = f_{rr}(0) = 0.2616$
$f_{yy} = f_{\theta\theta}(0) = 1$
$f_{xy} = f_{r\theta}(0) = 0.2083$

In Fig. 7, the distribution of the interfacial stresses obtained from both the finite element analysis and the theoretical model given in Eq 6 is plotted for a small range near the singular point.

It is seen that drastic stress intensification occurs near the free surface edge. Approaching the singular point, the magnitude of the stress rapidly increases further. But in real materials, it is thought that the stress would not go to infinity at the free surface (Ref 24).

In the case of the normal component σ_{yy}, a good agreement between the two curves is found in the given region. Figure 7 indicates that the theoretical model presented above can predict the stress state near the singular point.

The variation of this stress intensity factor K under the HHF load given in Fig. 3 is shown in Fig. 8. The results for the transient HHF loading are compared to those for the uniform heating case. A discrepancy of the two curves is found in the vicinity of the load-off point (t = 2 s) where the maximum temperature gradient develops in the joint. The maximum relative difference between the two load cases is about 6.9%.

Under the HHF load, the thermal deformation near the stress singularity causes higher stressing than the isothermal deformation. This is due to the forced axial bending generated by the temperature gradient under HHF load. The unit of the stress intensity factor is the same as that of the stress, because the coordinate in Eq 6 is normalized. The tendency of the curve variations in Fig. 8 is similar to that in Fig. 4, which indicates

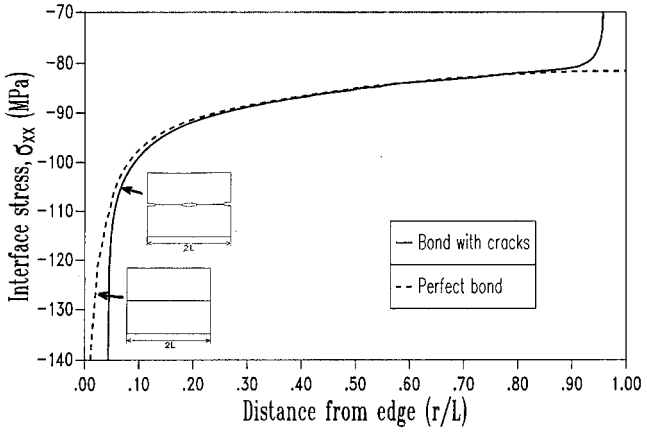

(a)

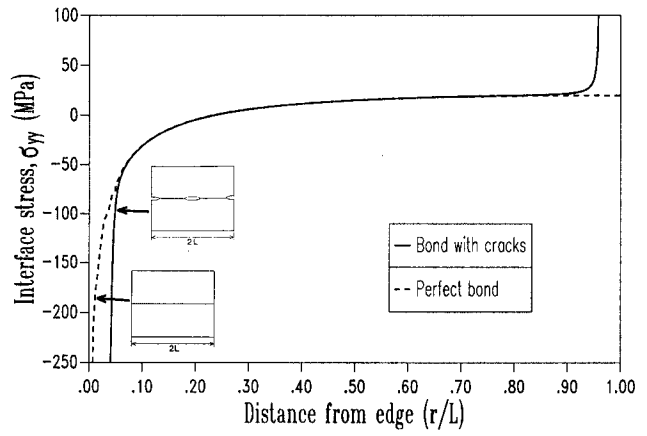

(b)

Fig. 5 Distribution of the residual stress in the perfect interface and in the cracked bond interface. (a) Axial stress component σ_{xx}. (b) Normal stress component σ_{yy}

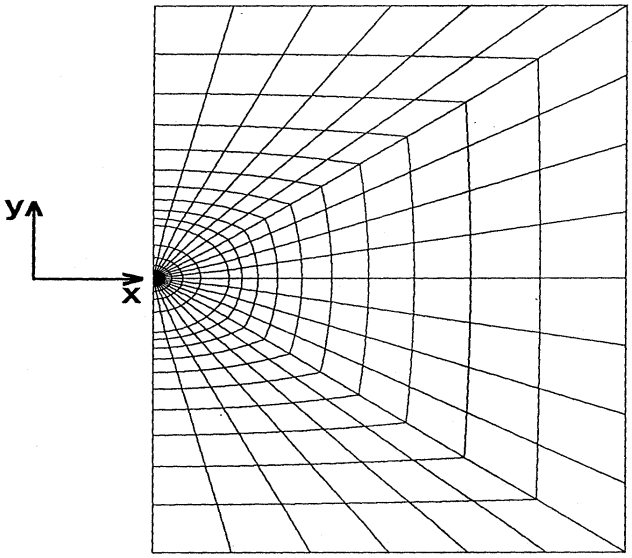

(a)

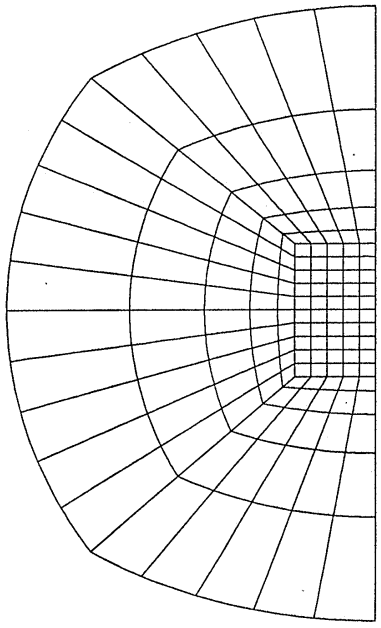

(b)

Fig. 6 Finite element mesh used to calculate the singular stress fields. (a) Mesh for the whole geometry. (b) Mesh for the singular region

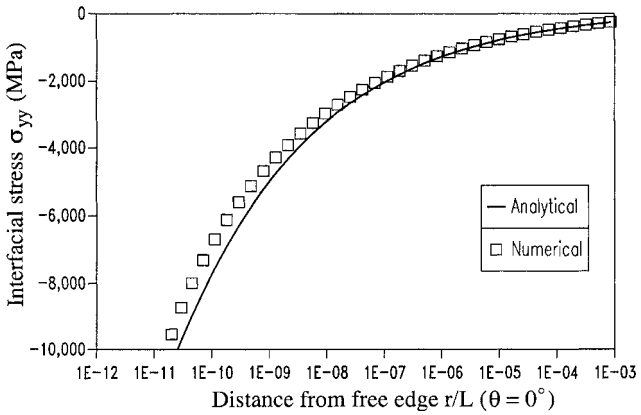

Fig. 7 Distribution of the interfacial stresses near the free edge of the interface (normal stress component σ_{yy})

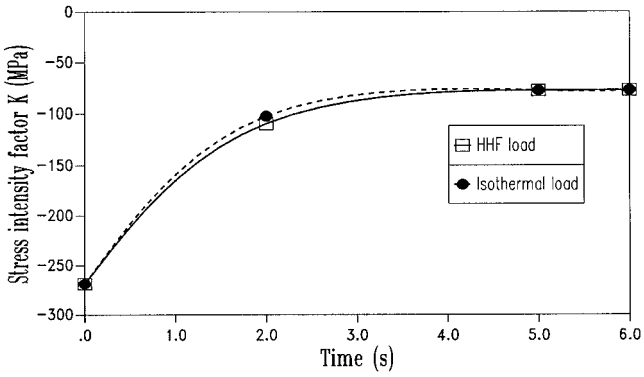

Fig. 8 Variation of the stress intensity factor *K* for the stress singularity at the interface edge

that the behavior of the singular edge stress fields has a qualitative pattern similar to that of the bulk stresses.

5. Summary

The duplex bond joint consisting of a metallic substrate armored with carbon-base materials is a promising candidate configuration for application to high heat flux operations.

When a bond joint is subjected to thermal loadings, significant thermal stresses may develop due to mismatch of the thermal expansion coefficients. Stress intensification occurs near the free surface edge of the interface, sometimes showing singularity. The interfacial stress fields are important for understanding the loading nature of a bond joint and may be a critical factor in structural integrity.

In this paper, thermal stresses in the bond interface of a carbon-to-molybdenum bond element were investigated. The temperature and stress fields were calculated using a finite element method. A high heat flux pulse was assumed as the reference load history to simulate the thermal shock condition.

The numerical result of bulk stress is compared to the prediction from Timoshenkos beam theory. There was some discrepancy between the numerical results and the values from the beam theory ranging from approximately 12.5 to 25%.

Drastic stress intensification occurred near the free surface edge. The transient behavior of the singular stress fields was described quantitatively in terms of the stress intensity factor. It was shown that Yang's formulation could describe the singular stress fields in a good approximation, even for the non-harmonic temperature fields caused by transient thermal load.

The stress intensity factor of the singular stress fields near the free surface edge of the interface showed a time variation similar to that of the bulk stress. The temperature gradient induced by the transient HHF load affected the overall interfacial stress only slightly.

References

1. M. Araki, M. Akiba, M. Dairaku, K. Iida, H. Ise, M. Seki, S. Suzuki, and K. Yokoyama et al., Thermal Response of Bonded CFC/OFHC Divertor Mock-ups for Fusion Experimental Reactors under Large Numbers of Cyclic High Heat Loads, *J. Nucl. Sci. Tech.*, Vol 29, 1992, p 901-908
2. S. Deschka, A. Cardella, J. Linke, M. Lochter, and H. Nickel, High Heat Flux Performance of Actively Cooled Divertor Mock-ups, *J. Nucl. Mater.*, Vol 203, 1993, p 67-72
3. Y. Yoshino, H. Ohtsu, and T. Shibata, Thermally Induced Failure of Copper-bonded Alumina Substrates for Electronic Packaging, *J. Am. Ceram. Soc.*, Vol 75, 1992, p 3353-3357
4. R. Kußmaul, "Einfluß Unterschiedlicher Fügeflächengeometrien auf die Eigenspannungen und die Festigkeit von Gelöteten Keramik-Metall-Verbunden," Ph.D. Thesis, University of Karlsruhe, Karlsruhe, Germany, 1994 (in German)
5. J.M. McNaney, R.M. Cannon, and R.O. Ritchie, Near-interfacial Crack Trajectories in Metal-Ceramic Layered Structures, *Int. J. Fracture*, Vol 66, 1994, p 227-240
6. M.D. Drory, M.D. Thouless, and A.G. Evans, On the Decohesion of Residually Stressed Thin Films, *Acta Metall.*, Vol 36, 1988, p 2019-2028
7. S. Timoshenko, Analysis of Bi-metal Thermostats, *J. Opt. Soc. Am.*, Vol 11, 1925, p 233-255
8. O. Iancu, "Berechnung von Thermischen Eigenspannungsfeldern in Keramik/Metall-Verbunden," Ph.D. Thesis, University of Karlsruhe, Karlsruhe, Germany, 1989 (in German)
9. J.D. Whitcomb, I.S. Raju, and J.G. Goree, Reliability of the Finite Element Method for Calculating Free Edge Stresses in Composite Laminates, *Comput. Struct.*, Vol 15, 1982, p 23-37
10. B.J. Dalgleish, M.C. Lu, and A.G. Evans, *Acta Metall.*, Vol 36, 1988, p 2029-2035
11. K. Kokini and R.W. Perkins, Free Edge Thermal Stress Singularities in Finite Concentric Cylinders, *Comput. Struct.*, Vol 19, 1984, p 531-534
12. R. Viola and E.B. Deksnis, Geometry Free of Singularities for Fusion Duplex Components, JETP Lett., Vol 94, 1994, p 54
13. M.L. Williams, The Stresses around a Fault or Crack in Dissimilar Media, *Bull. Seismol. Soc. Am.*, Vol 49, 1959, p 199-204
14. D.B. Bogy, Edge-bonded Dissimilar Orthogonal Elastic Wedges under Normal and Shear Loading, *Trans. ASME, J. Appl. Mech.*, Vol 35, 1968, p 460-466
15. S.S. Wang and I. Choi, Boundary-layer Effects in Composite Laminates, *Trans. ASME, J. Appl. Mech.*, Vol 49, 1982, p 541-560
16. K. Mizuno, K. Miyazawa, and T. Suga, Characterization of Thermal Stresses in Ceramic/Metal Joint, *J. Fac. Eng., Univ. Tokyo (B)*, Vol 39, 1988, p 401-412

17. J.P. Blancard and N.M. Ghoniem, Relaxation of Thermal Stress Singularities in Bonded Viscoelastic Quarter Planes, *Trans. ASME, J. Appl. Mech.*, Vol 56, 1989, p 756-762

18. D. Munz and Y.Y. Yang, Stress Singularities at the Interface in Bonded Dissimilar Materials under Mechanical and Thermal Loading, *Trans. ASME, J. Appl. Mech.*, Vol 59, 1992, p 857-861

19. D. Munz, T. Fett, and Y.Y. Yang, The Regular Stress Term in Bonded Dissimilar Materials after a Change in Temperature, *Eng. Frac. Mech.*, Vol 44, 1993, p 185-194

20. J.P. Blancard and N.M. Ghoniem, Analysis of Singular Stress Fields in Duplex Fusion Components, *J. Nucl. Mater.*, Vol 172, 1990, p 54-70

21. M. Fränkle, D. Munz, and Y.Y. Yang, Stress Singularities in a Bimaterial Joint with Inhomogeneous Temperature Distribution, *Int. J. Solid Struct.*, Vol 33, 1996, p 2039-2054

22. *ABAQUS User's Manual 5.4*, Hibbit, Karlson and Sorenson Inc., Providence, RI, 1994

23. I. Smid, M. Akiba, M. Araki, S. Suzuki, and K. Satoh, "Material and Design Considerations for the Carbon Armored ITER Divertor," JAERI-M 93-149, Japan Atomic Energy Research Institute, 1993

24. D. Post, J.D. Wood, B. Han, V.J. Parks, and F.P. Gerstle, Jr., Thermal Stresses in a Bimaterial Joint: An Experimental Analysis, *Trans. ASME, J. Appl. Mech.*, Vol 61, 1994, p 192-198